THE JOURNAL OF PHYSICAL CHEMISTRY C

C: Plasmonics; Optical, Magnetic, and Hybrid Materials

Achieving Conformational Control in RTP and TADF Emitters by Functionalization of the Central Core

Nadzeya A. Kukhta, Rongjuan Huang, Andrei S. Batsanov, Martin R. Bryce, and Fernando B. Dias

J. Phys. Chem. C, **Just Accepted Manuscript** • DOI: 10.1021/acs.jpcc.9b08238 • Publication Date (Web): 04 Oct 2019

is published by the American Chemical Society. 1155 Sixteenth Street N.W., Washington, DC 20036

Achieving Conformational Control in RTP and TADF Emitters by Functionalization of the Central Core

Nadzeya A. Kukhta,[a†]* Rongjuan Huang,[b†] Andrei S. Batsanov,[a] Martin R. Bryce,[a,]*

Fernando B. Dias [b,]*

[a]*Department of Chemistry, Durham University, South Road, Durham, DH1 3LE, UK*

[b]*Department of Physics, Durham University, South Road, Durham, DH1 3LE, UK*

Abstract

Three new symmetrical donor–acceptor–donor (D–A–D)-type molecules were prepared with phenothiazine (PTZ) as electron donors and 9,9-dimethylthioxanthene (TX) as the electron acceptor. The PTZ groups are attached at different positions on the acceptor core – *ortho* or *meta* to the sulfur of TX. The molecules have been characterized by X-ray crystallography, in-depth photophysical studies and theoretical calculations. This series provides new insights into how molecular functionalization and intramolecular charge transfer determines the singlet-triplet gap ΔE_{ST}. Two of the molecules have weak D/A decoupling and a relatively large ΔE_{ST} of 0.52 eV which prohibits the upconversion of triplet excitons to the singlet state, showing strong room temperature phosphorescence (RTP). When the TX acceptor strength is enhanced by the attachment of benzoyl substituents a very small ΔE_{ST} of <0.01 eV is observed. In this case excitons in the triplet state can be efficiently upconverted to the singlet state *via* reverse intersystem crossing (RISC) resulting in thermally activated delayed fluorescence (TADF). TADF and RTP are unambiguously assigned by distinctive photophysical data, notably a comparison of degassed and aerated luminescence spectra, temperature-dependent time-resolved fluorescence decays and power dependence of the intensity of delayed emission (for the TADF emitter).

Introduction

Nowadays, a manifold of fluorescent emitters has been developed for optoelectronic applications including organic light emitting diodes (OLEDs),[1–5] sensing,[6,7] probes for fluorescent imaging[8] and optical thermometry.[9] However, most of the emitters employed in the above-mentioned applications follow the singlet decay channel only, which limits dramatically the electroluminescence efficiency in devices.[10–12] Phosphorescent emitters based on complexes containing transition metals such as iridium and platinum offer metal-ligand charge transfer (MLCT) states to facilitate spin-orbit coupling (SOC) which enables the utilization of both singlet and triplet excitons.[13–15] However, the use of metal-based phosphorescent emitters is cost-inefficient due to the scarcity and cost of noble metals. Moreover, these complexes suffer from instability in some practical applications.[16] Photoluminescence efficiencies close to 100% can be achieved using only the singlet state. Therefore, the main advantages of harvesting triplets in photoluminescence applications comes from achieving longer luminescence lifetimes that can be beneficial for some applications including oxygen sensing, imaging and anti-counterfeit labelling, for example.

An alternative way to harvest both singlet and triplet excited states is based on thermally activated delayed fluorescence (TADF), which currently is the leading strategy offering internal quantum efficiency (IQE) of 100% in electroluminescent diodes using purely organic (metal-free) emitters.[17–20] Mechanistically, TADF differs from phosphorescence, as the long-lived emission appears from the singlet state, following the up-conversion of triplet states into emissive singlets due to thermally assisted reverse intersystem crossing (RISC).[21–23] For efficient TADF to occur the following requirements must be satisfied simultaneously: 1) well-decoupled donor (D) and acceptor (A) chromophores of similar electron donating/accepting strength and close triplet levels to ensure negligible ΔE_{ST}; 2) control of the D–A twist angle while retaining dynamic rocking at the D–A bond;[24] 3) conformational stability and 4) high photoluminescence quantum yield (PLQY). Various emission color TADF molecules have been realized.[5,25–29]

Long-lived phosphorescence is also observed in metal-free organic compounds occurring directly via triplet states. Typically, if delayed fluorescence is efficient, phosphorescence is weak because the RISC rate will quench the triplet population. Even though the emission from triplet states is highly sensitive to temperature, rigidity of the medium, and to the presence of molecular oxygen, efficient room temperature phosphorescence (RTP) can be realized when the molecular vibrations causing non-radiative $T_1 \rightarrow S_0$ relaxations are suppressed and efficient intersystem crossing (ISC) from S_1 to T_1 is promoted.[30,31] While RTP has been reported in hydrocarbon molecules containing heteroatoms (halogens, sulfur, oxygen) upon dispersion in polystyrene or in the cycloolefin polymer zeonex, or upon crystallization,[32] the molecular design strategies for all-organic RTP emitters are still quite limited.[33,34] The concept of using intramolecular charge transfer (ICT) states instead of MLCT states is similar for obtaining TADF and organic RTP, although ΔE_{ST} should be much larger for RTP than for TADF in order to suppress RISC and shift the equilibrium to the triplet state. It is important to ensure that the large ΔE_{ST} does not affect the triplet formation yield.

In the majority of the reported RTP systems based on D–A molecules triplet emission was observed only in specific conformers or regioisomers. For example, when a phenothiazine (PTZ) donor was employed in the emitters, the PTZ planarized axial (*ax*) conformers were mainly responsible for decaying via RTP,[31,35,36] whereas the PTZ equatorial (*eq*) form mostly decays via TADF. Moreover, conformational disorder leads to the loss of radiative pathways as well as to detrimental dual photoluminescence.[37–39] Due to the potential for conformational disorder the PTZ donor can lead to complicated structural and photophysical properties even though it has the benefit of greatly enhancing the ISC rate.[31] The tendency for conformational disorder (quasi-*ax* and quasi-*eq* forms) was also detected for a functionalized dihydroacridine donor, which is generally considered to be a rigid chromophore.[40] Thus, the need exists for more detailed investigations of structure-property relationships in these types of D–A molecules, including an additional focus on the conformational analysis, for the rational design of TADF and RTP emitters.

The current work presents a new molecular design approach aimed at preventing the formation of multiple axial (*ax*) and equatorial (*eq*) conformers while employing the PTZ donor in a D–A–D system with the thioxanthene (TX) acceptor unit. By introducing *tert*-butyl substituents onto the TX acceptor and altering the linking position of the PTZ moiety (*ortho*- *vs*. *meta*- relative to the sulfur atom of TX) efficient RTP emitters with solely *eq*

conformation were obtained. Moreover, functionalization of the TX fragment with benzoyl groups resulted in a negligible ΔE_{ST}, enhanced RISC rate and efficient yellow TADF. The motivation was to understand the impact of the internal conformers of PTZ on the resulting TADF and RTP properties of D–A–D emitters. To the best of our knowledge, this is the first detailed study on the differences between the internal (within the PTZ unit) conformers, as opposed to the widely studied[41,42] *ax/eq* conformers that form due to the rotation around the D–A bond.

Results and discussion

Molecular design

The new molecules studied in this work are shown in **Chart 1**. It is well-known that the presence of heteroatoms such as sulfur and oxygen is beneficial for increasing the ISC/RISC rates of RTP and TADF emitters.[31,32,35] Phenothiazine is thus popular as an electron-donor component in this context.[31,35,37,43] Heterocycles featuring sulfur in various valence states have also been investigated as electron accepting fragments due to their strong triplet yield.[19,44] Furthermore, molecular orientation of the structural moieties within the molecule plays a crucial role in promoting or interrupting the conjugation, thus influencing the vibronic coupling.[23] As shown previously[35,42] enhancing the steric hindrance adjacent to the D–A bond by substituting either D or A units with bulky groups decouples the chromophores, transforming efficient TADF emitters into RTP emitters. Nevertheless, changes in the RTP/TADF properties may be expected not only due to the functionalization of the D and A fragments, but also due to a change in the linking pattern. Hence, the rationale behind the design on the molecules in this study includes: 1) prevention of the radiationless processes caused by multiple conformers by means of locking the molecule solely in one conformation; 2) probing the dependence of RTP characteristics on the linking pattern; 3) switching on the TADF property by enhancing the electron accepting strength of the core unit. The first two points were addressed by introducing sufficient steric hindrance (*t*-butyl group in *para*-positions to the sulfur of TX) and attaching the PTZ donors to *meta*- and *ortho*- positions of the core (**Chart 1**), thus enhancing the rotation barrier. The third point was tackled by introducing carbonyl groups onto the electron-accepting TX unit leading to extensive HOMO/LUMO redistribution, negligible ΔE_{ST} and efficient TADF.

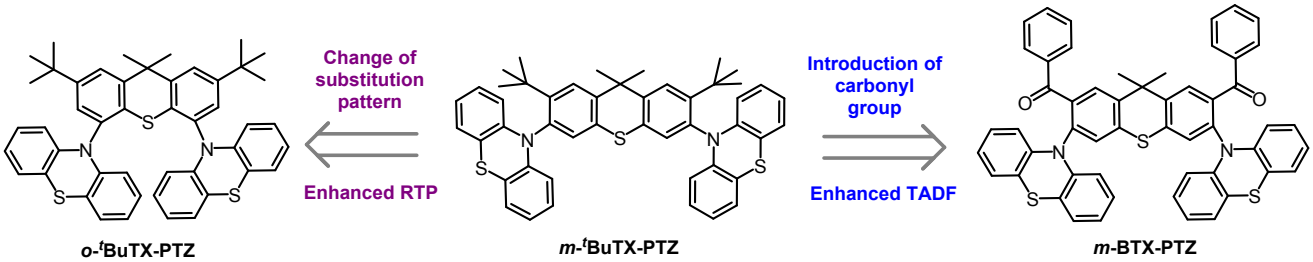

Chart 1. Chemical structures of ***o*-^{t}BuTX-PTZ**, ***m*-^{t}BuTX-PTZ** and ***m*-BTX-PTZ**. (*Ortho*- and *meta*- refer to the substitution position of the phenothiazinyl units relative to the sulfur atom of TX).

All the studied compounds were obtained by multistep synthetic procedures which are described in the SI. Buchwald-Hartwig coupling was employed at the main step for linking the D and A units.[45] The identity and purity of the target molecules were unambiguously

proved by a combination of NMR spectroscopy, mass spectrometry and elemental analysis. Thermal stability was probed by thermal gravimetric analysis (TGA) (**Figure S1**, Section S1).

X-Ray crystallography.

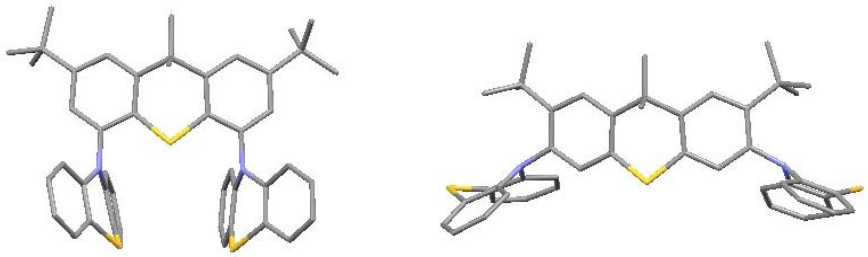

Figure 1. X-Ray structures of ***o*-^{t}BuTX-PTZ** and ***m*-^{t}BuTX-PTZ** (hydrogen atoms are omitted).

In the crystal structure of ***o*-^{t}BuTX-PTZ**, the 2,7-di-*tert*-butyl-9,9-dimethyl-9*H*-thioxanthene (TX) unit is folded by 39.4° along the S…C(Me_2) vector and both phenothiazine (PTZ) donors adopt equatorial conformations with near-orthogonal twists (89° and 80°) about the connecting C-N bonds (Section S3, **Table S1**). Both PTZ moieties are folded along the S…N vectors by 25.3° and 35.5°, their sulfur atoms are bent inward (*syn*-orientation), so that the S…S distance (4.10 Å) is much shorter than the N…N distance (5.23 Å), although still longer than a close van der Waals contact (3.6-3.7 Å). Two PTZ arene rings contact almost face-to-face with the interplanar angle of 22°. ***m*-^{t}BuTX-PTZ** was studied in two crystal forms, the non-solvated orthorhombic and the triclinic DCM solvate, the latter containing two symmetrically independent molecules. The molecular conformations are similar: the TX unit is folded by 38-39° and the PTZ units by 31-40°, the PTZ conformation is equatorial with a 85-90° twist with respect to the TX. Interestingly, in each case the PTZ units are folded outwards (*anti*-orientation) rather than inwards (*syn*-orientation), as in the *o*-isomer. Crystals of ***m*-BTX-PTZ** suitable for X-ray analysis could not be obtained.

Theoretical calculations.

The optimized ground state geometry of the target phenothiazine (PTZ) derivatives was accessed at the rBMK/6-31G(d) level of theory (42% HF)[46,47] which has proved to be suitable for the description of electronic processes in linked donor–acceptor systems[48,49] (**Figure 2**). Interestingly, in all three derivatives, namely ***o*-^{t}BuTX-PTZ**, ***m*-^{t}BuTX-PTZ** and ***m*-BTX-PTZ**, the central TX moiety has a planar molecular skeleton, which obviously differs from the X-ray crystal structures (**Figure 1**). This divergence can originate from the differences between gas phase calculations[50] and crystal packing. The folded PTZ donors (α = 36-40°) are attached nearly orthogonally (79.7-84°) to the central core, regardless of the nature and position of the core substituents. Interestingly, the orientation of the PTZ unit seems to be

dependent on the position of the substituents on the TX acceptor. In the case of ***o*-^{t}BuTX-PTZ** the PTZ units are folded towards each other in a *syn*-conformation, while in ***m*-^{t}BuTX-PTZ** and ***m*-BTX-PTZ** the donors have *anti*-orientation. These observations which are in agreement with the X-ray results (**Figure 1**) inspired us to study conformational isomerism of the PTZ derivatives, focusing only on the internal orientation of the PTZ unit (the details can be found in the SI).

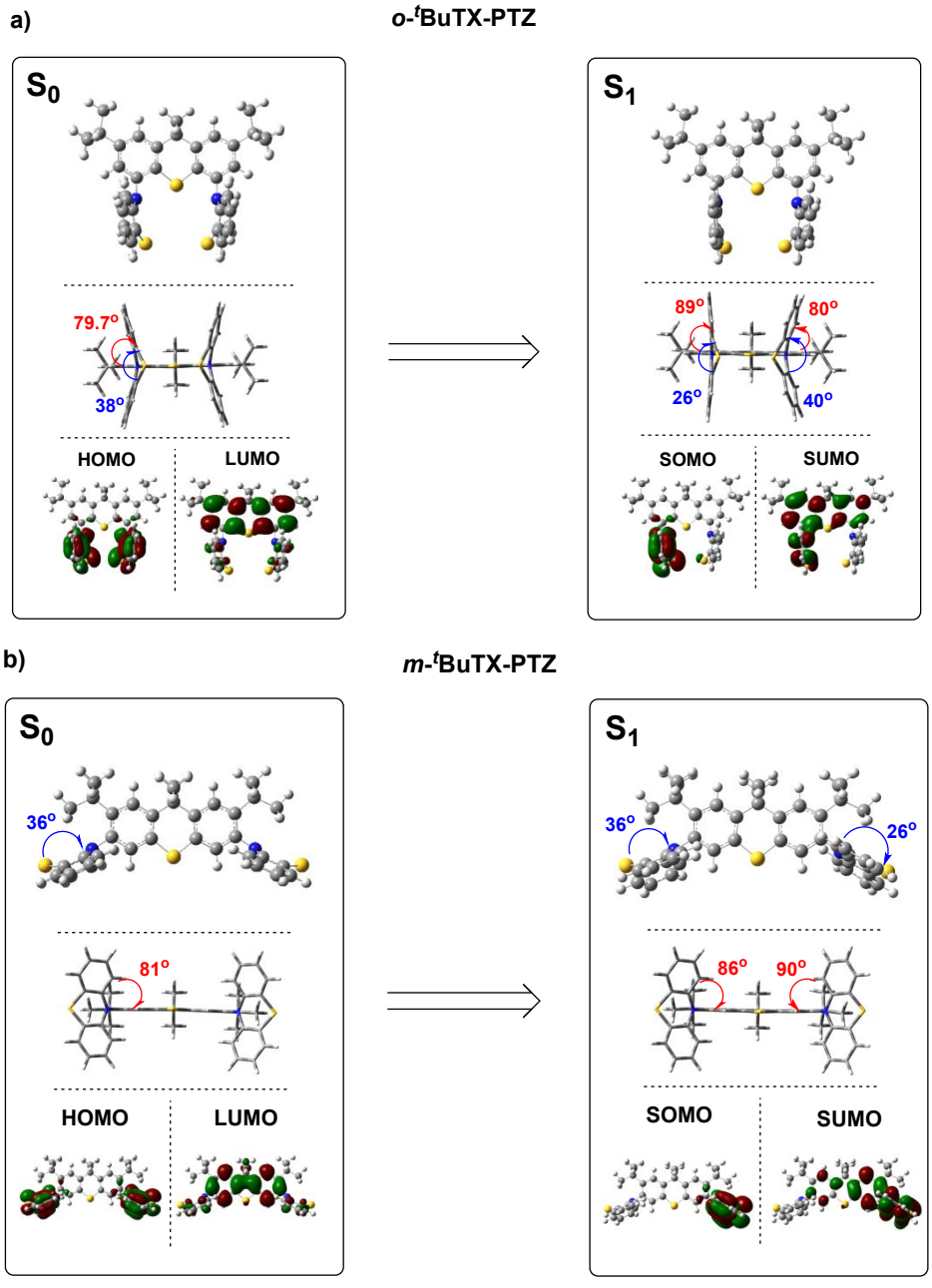

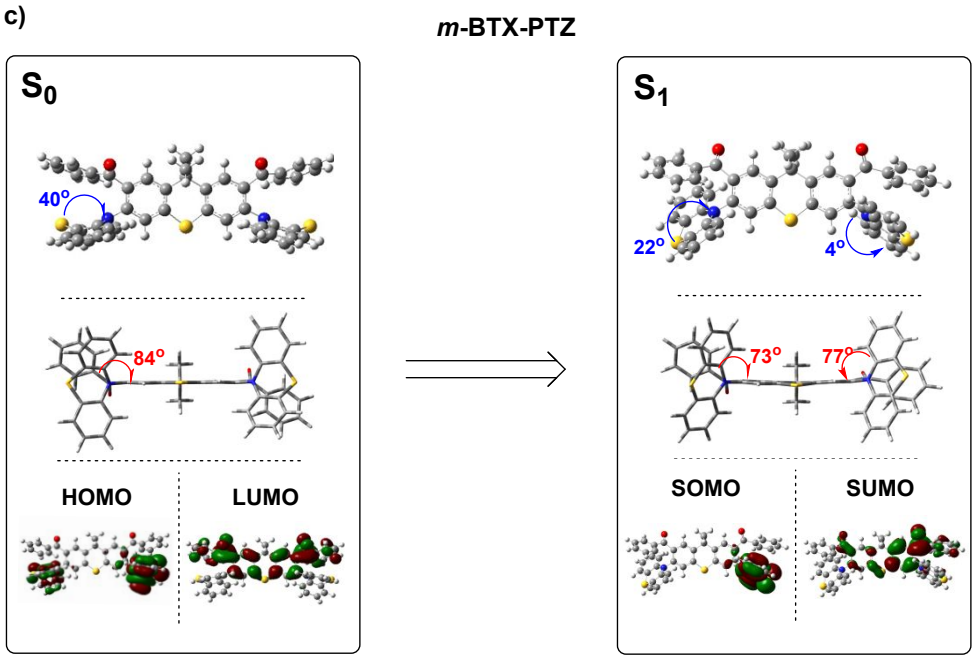

Figure 2. Minimum energy ground state (rBMK/6-31G(d)) and first singlet excited state (TDA-DFT BMK/6-31G(d)) optimized structures along with the frontier orbitals of (a) ***o*-^{t}BuTX-PTZ**, (b) ***m*-^{t}BuTX-PTZ** and (c) ***m*-BTX-PTZ**. SOMO corresponds to Singly Occupied Molecular Orbital; SUMO corresponds to Singly Unoccupied Molecular Orbital.[51]

It is noteworthy that core substituents on the one hand, and *ortho*-substitution on the other hand, create sufficient steric hindrance to lock the molecule in the equatorial conformation and to prevent the formation of the planarized axial conformer, which has been shown to be detrimental to the TADF properties of many PTZ-based materials due to the enhanced conjugation, leading to LE/CT mixing and, hence, to the appearance of dual emission.[35,52] In order to confirm the stability of the equatorial conformation, the total energy scans visualizing the dependence of the conformational energy on the value of the D–A angle twist were calculated (**Figure 3**). The geometry of the conformers was optimized at each step. High energy of up to 1 eV is required to twist the PTZ donor by 60° relative to the plane of the TX acceptor. Of note, the energy barrier becomes much higher for the *meta*-substituted derivatives with the higher twist angle (>60°) pointing at a higher degree of steric hindrance in ***m*-^{t}BuTX-PTZ** and especially ***m*-BTX-PTZ** featuring even more sterically bulky benzoyl fragments.

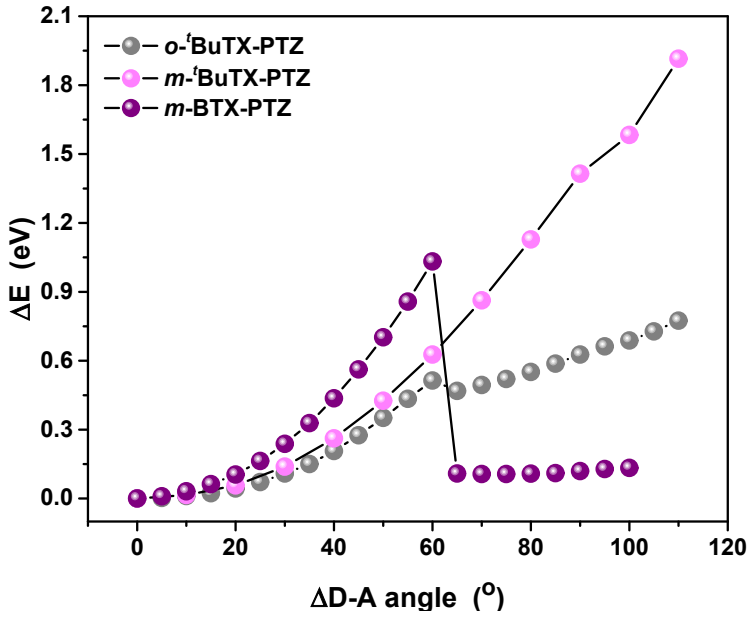

Figure 3. The dependence of the conformational energy of ***o*-^{t}BuTX-PTZ**, ***m*-^{t}BuTX-PTZ** and ***m*-BTX-PTZ** on the value of the D-A angle twist (rBMK/6-31G(d))

The conformers of the studied compounds at minimum energy (**Figure 2**) clearly possess different HOMO/LUMO energy values and wave function distribution. Thus, while in *ortho*-substituted ***o*-^{t}BuTX-PTZ** the HOMO is localized strictly on the PTZ donors, small delocalization onto the adjacent phenyl rings can be observed for the HOMO of ***m*-^{t}BuTX-PTZ**. The LUMO of both molecules is delocalized due to the weak electron-accepting ability of 2,7-di-*tert*-butyl-9,9-dimethyl-9*H*-thioxanthene (^{t}BuTX) when compared to the donating strength of PTZ. Noteworthy, the HOMO energy value is slightly higher when *ortho*-substitution is employed (-5.47 eV for ***o*-^{t}BuTX-PTZ** *vs* -5.68 eV for ***m*-^{t}BuTX-PTZ**) meaning that PTZ acts as a stronger electron donor when attached in the *ortho*-position. In turn, drastic redistribution of HOMO/LUMO wavefunctions takes place when the *t*-butyl substituents on the TX core are replaced by benzoyl groups in ***m*-BTX-PTZ**. While the HOMO is still mainly governed by the PTZ unit, the LUMO is now delocalized over the 9,9-dimethyl-9*H*-thioxanthene-2,7-diyl)bis(phenylmethanone) part. Thus, the electron-withdrawing nature of the carbonyl groups turns the TX core into a significantly stronger acceptor, lowering E_{LUMO} (-1.14 eV) and leading to good D/A decoupling. The cyclic voltammetry (CV) measurements also confirm this scenario as shown in **Figure S5** and **Table S3**. Furthermore, while only a single reversible oxidation peak is observed for the *meta*-substituted ***m*-^{t}BuTX-PTZ** and ***m*-BTX-PTZ**, interestingly, two reversible oxidation processes are detected for ***o*-^{t}BuTX-PTZ**. We tentatively attribute the appearance of the second peak to the additional through-space interaction of the phenothiazine donors induced by *ortho*-substitution. This is comparable to the case of cofacially stacked dihydrodiazapentacene donors, where the large splitting between the oxidation potentials was explained by two, sequential one-electron oxidation process.[53]

The theoretically predicted UV-Vis absorption spectra (**Figure 4**) further highlight the differences between the molecules. Tamm-Dancoff approximation was exploited for the

simulation of the UV-Vis spectra due to more accurate description of the CT transitions compared to TD-DFT.[54,55] While the absorption spectra of ***o*-^{t}BuTX-PTZ** and ***m*-^{t}BuTX-PTZ** have vibronic shape and extend to 345-370 nm, the absorption of ***m*-BTX-PTZ** has a clear Gaussian shape and onset at 425 nm confirming the CT nature of this compound. Interestingly, the extinction coefficient of ***m*-^{t}BuTX-PTZ** is the highest within the series and the peak ratio differs from that of ***o*-^{t}BuTX-PTZ** (high energy peak at 232 nm is much higher in the case of ***m*-^{t}BuTX-PTZ**). We can potentially attribute these differences to the higher LE character in ***m*-^{t}BuTX-PTZ**. The above assumption is in line with the shape of the singlet natural transition orbitals (NTO)[56] of the derivatives (**Figure S3**): while both hole and particle are localized solely on the PTZ donor in the case of ***m*-^{t}BuTX-PTZ**, the particle features the U-shape involving both TX and PTZ moieties in ***o*-^{t}BuTX-PTZ**, implying a higher degree of charge transfer in the latter. The shape of the $S_0 \rightarrow S_{2,3}$ NTO (**Figure S3**) confirms that *ortho*-substitution leads to stronger CT. On the contrary, the significant extent of hole/particle localization retained in $S_0 \rightarrow S_{1,2}$ excitations of ***m*-BTX-PTZ** proves much stronger CT in this compound when compared to the ^{t}Bu derivatives ***o*-^{t}BuTX-PTZ** and ***m*-^{t}BuTX-PTZ**.

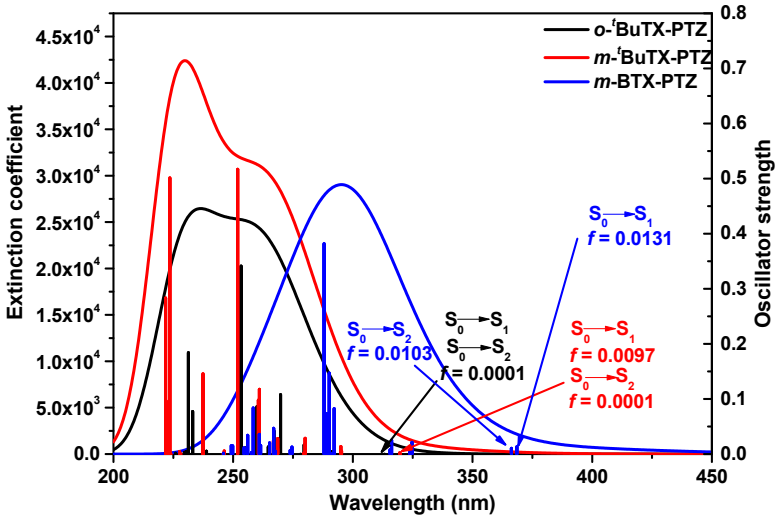

Figure 4. Theoretically predicted absorption spectra of the minimum energy conformers of ***o*-^{t}BuTX-PTZ**, ***m*-^{t}BuTX-PTZ** and ***m*-BTX-PTZ** (TDA-DFT rBMK/6-31G(d)).

The values of the triplet levels of ***o*-^{t}BuTX-PTZ**, ***m*-^{t}BuTX-PTZ** and ***m*-BTX-PTZ** were accessed (TDA-DFT rBMK/6-31G(d), **Figure 5**). While the T_1 values are very similar for ***o*-^{t}BuTX-PTZ** and ***m*-^{t}BuTX-PTZ** (3.44 and 3.35 eV, respectively), the triplet level of ***m*-BTX-PTZ** is slightly lower (3.18 eV) due to the electron withdrawing benzoyl groups. It is noteworthy that the introduction of the carbonyls in ***m*-BTX-PTZ** leads to strong CT character (see NTOs, **Figure S3**), ensuring a much smaller gap between S_1 and T_1 (0.18 eV) compared to ***o*-^{t}BuTX-PTZ** and ***m*-^{t}BuTX-PTZ** (0.51 eV and 0.52 eV, respectively), suggesting that ***m*-BTX-PTZ** can be a TADF emitter. In turn, the observation of large $\Delta E_{S1\text{-}T1}$ promoted by a negligible S_1-T_n splitting[57] ($\Delta E_{S1\text{-}T5} = 0.011$ eV and $\Delta E_{S1\text{-}T3} = 0.054$ eV for ***o*-^{t}BuTX-PTZ** and ***m*-^{t}BuTX-PTZ**, respectively) leads to enhanced spin-orbit coupling. Tiny $\Delta E_{S1\text{-}Tn}$ values suggest that efficient ISC can be turned on in ***o*-^{t}BuTX-PTZ** and ***m*-^{t}BuTX-PTZ**, making them efficient RTP emitters.

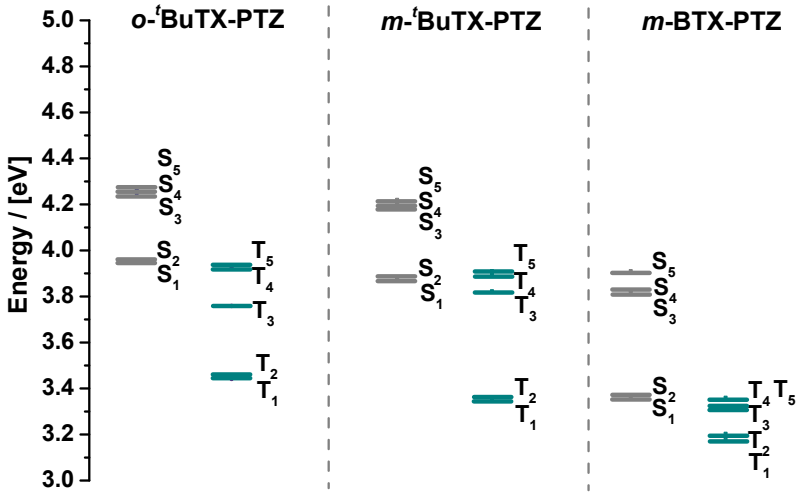

Figure 5. Singlet and triplet energy diagram of the minimum energy conformers of ***o*-^{t}BuTX-PTZ**, ***m*-^{t}BuTX-PTZ** and ***m*-BTX-PTZ** (TDA-DFT rBMK/6-31G(d)).

In the first excited state S_1 (**Figure 2**) all the molecules of the series experience geometrical changes, leading to asymmetrical structures. In the case of ***o*-^{t}BuTX-PTZ** and ***m*-^{t}BuTX-PTZ**, the folding torsion angle of one of the PTZ units decreases from 40º to 26º while gaining solely perpendicular orientation relative to the plane of the acceptor (89-90º). In turn, ***m*-BTX-PTZ** undergoes more pronounced PTZ donor planarization (22º and 4º) with a slight decrease in the D–A angles (73-77º). These observations can be attributed to the hybridization of the nitrogen atom of the PTZ unit, which changes upon electronic excitation. In the case of complete electron withdrawal, the nitrogen atom can adopt a planar configuration.[58,59] The latter is clearly detected in ***m*-BTX-PTZ** due to the presence of electron accepting benzoyl groups and stronger CT character. Partial planarization of the singular PTZ donor results in a change in chromophore communication: the SOMO (Singly Occupied Molecular Orbital) tends to be localized over the planarized PTZ, while the SUMO (Singly Unoccupied Molecular Orbital) is delocalized over the D–A fragment, excluding the second donor. Of note, ***m*-BTX-PTZ** retains good SOMO/SUMO decoupling even in the excited state.

To gain an additional insight into the nature of the T_1 states, the geometry of the first triplet state was optimized (**Figure 6**). Similarly to the S_1 state, all the molecules favor an asymmetrical configuration. While the geometry and corresponding SOMO/SUMO distribution for the triplet state of ***o*-^{t}BuTX-PTZ** is very similar to that of the S_1 state (**Figure 2**), only one donor experiences partial planarization in ***m*-BTX-PTZ** (9º). The latter is involved in the SOMO/SUMO wavefunction distribution of a mixed π-π*/n-π* character. However, an unusual situation is observed in the T_1 optimized structure of ***m*-^{t}BuTX-PTZ**. While the optimized structures of all the molecules in the S_0 and S_1 states, and of ***o*-^{t}BuTX-PTZ** and ***m*-BTX-PTZ** in the T_1 state, feature a planar TX acceptor unit, a crooked TX motif is observed in the T_1 state of ***m*-^{t}BuTX-PTZ** (similar to the X-ray structure, **Figure 1**). Along with the partially planarized and twisted PTZ donor, the folding of the central unit leads to

the high LE character of the T_1 state. On the contrary, the delocalized T_1 SOMO/SUMO of the *ortho*-substituted compound ***o*-^{t}BuTX-PTZ** implies a higher percentage of the π-π* character in the hybrid π-π*/n-π* orbitals. This orbital character was shown to be a crucial criterion for the enhanced ISC rate in persistent RTP emitters.[57] Thus, even though ***o*-^{t}BuTX-PTZ** and ***m*-^{t}BuTX-PTZ** exhibit similar features in the S_0 and S_1 states (geometry, UV-Vis absorption spectra), the tilted skeleton of ***m*-^{t}BuTX-PTZ** in the T_1 state can explain the differences in triplet emission.

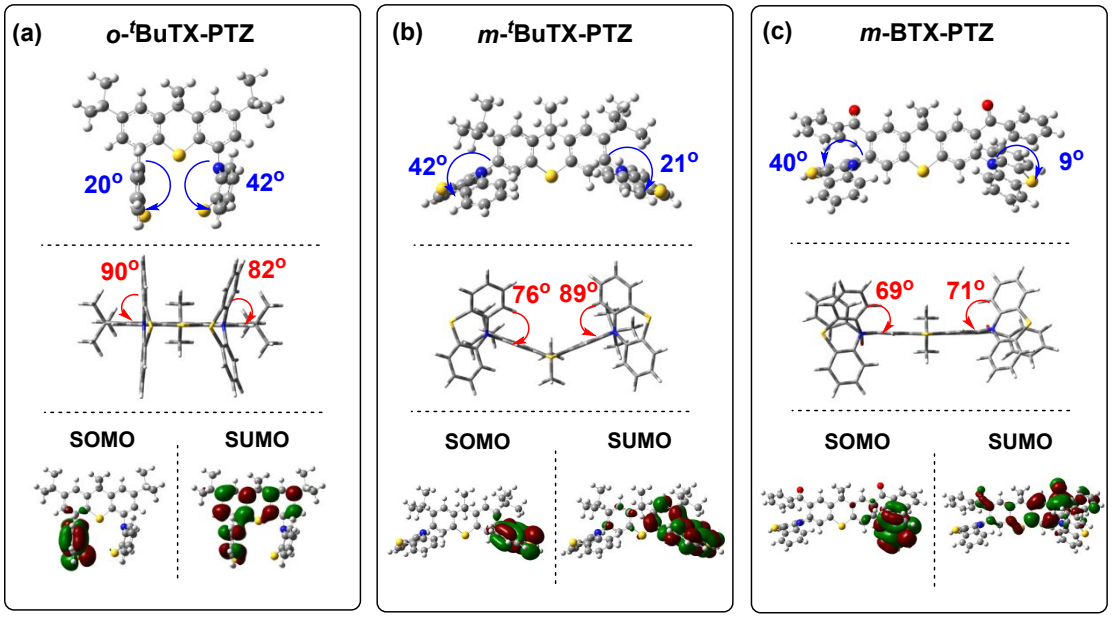

Figure 6. First triplet (T_1) excited state (TDA-DFT BMK/6-31G(d)) optimized structures and the frontier orbital maps of (a) ***o*-^{t}BuTX-PTZ**, (b) ***m*-^{t}BuTX-PTZ** and (c) ***m*-BTX-PTZ**. SOMO corresponds to Singly Occupied Molecular Orbital; SUMO corresponds to Singly Unoccupied Molecular Orbital.

The relative planarization of the PTZ donor in the excited states (S_1 and T_1) proves that the existence of *syn/anti* conformers is solely a ground state feature which has a moderate impact on the ground state properties. However, this feature can be ignored in the investigation of the excited state characteristics. Thus, PTZ can be further involved in the design of efficient RTP and TADF emitters when the dual emission (*ax/eq*) is suppressed.

Optical and photophysical characteristics

Absorption and Photoluminescence Properties

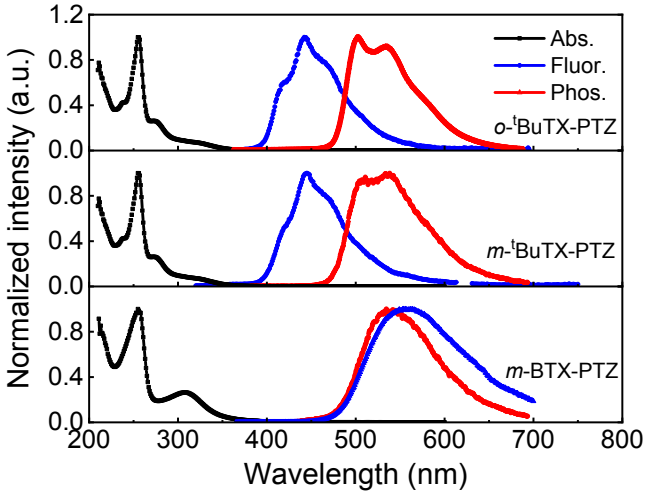

Figure 7. Normalized absorption spectra (black) of ***o*-^{t}BuTX-PTZ**, ***m*-^{t}BuTX-PTZ** and ***m*-BTX-PTZ** measured in diluted MCH (1.0×10^{-4} M) at room temperature, fluorescence (blue) and phosphorescence (red) spectra in zeonex matrix (1 wt%) collected at room temperature and 80 K, respectively.

Figure 7 shows the normalized UV-Vis absorption and photoluminescence (PL) spectra of ***o*-^{t}BuTX-PTZ**, ***m*-^{t}BuTX-PTZ** and ***m*-BTX-PTZ**. All the compounds exhibit higher energy absorption bands around 250 nm, which can be attributed to a π-π* transition. Similar weak absorption tails with onsets at *ca.* 350 nm are observed in both ***o*-^{t}BuTX-PTZ** and ***m*-^{t}BuTX-PTZ**, whereas ***m*-BTX-PTZ** shows a broad absorption band peaking at 312 nm showing a CT character.

Clear and defined differences are observed in the emission behaviours. ***o*-^{t}BuTX-PTZ** shows a well-resolved fluorescence spectrum in zeonex film peaking at 450 nm, which is entirely independent of solvent polarity as depicted in **Figure S6a**. The phosphorescence spectrum also shows a characteristic vibrational structure, indicating its localized excited triplet (^{3}LE) character. The *meta*-substituted compound ***m*-^{t}BuTX-PTZ** exhibits similar well-resolved fluorescence and phosphorescence spectra as ***o*-^{t}BuTX-PTZ**, identifying their LE characters. Calculated from the onsets of their fluorescence spectra, the localized excited singlet (^{1}LE) energies of ***o*-^{t}BuTX-PTZ** and ***m*-^{t}BuTX-PTZ** are the same (3.12 eV), and are isoenergetic with that of the PTZ unit (**Figure S7**). Likewise, the triplet states of these two molecules are also close in energy (2.60 eV) and the phosphorescence spectra match well with that of PTZ, further indicating their localized character. Therefore, the singlet-triplet energy splitting (ΔE_{ST}) of both ***o*-^{t}BuTX-PTZ** and ***m*-^{t}BuTX-PTZ** is calculated to be 0.52 eV. This is consistent with the analysis of the hole-particle NTOs (**Figure S3**), which shows that both hole and particle NTOs of ***o*-^{t}BuTX-PTZ** and ***m*-^{t}BuTX-PTZ** are localized on the donor

units, due to their weak D–A electronic coupling. It is proposed that the substituted position of PTZ unit (*ortho*- and *meta*-) has no significant effect on the absorption and PL spectra.

In contrast, when the *tert*-butyl substituents on the TX unit in ***m*-^{t}BuTX-PTZ** are replaced by benzoyl groups, ***m*-BTX-PTZ** shows a broad and featureless emission peaking at 554 nm as shown in **Figure 7**. It is assigned to CT character in the singlet excited state, which is further confirmed by the red shift which occurs with increasing solvent polarity (**Figure S6c**). The ^{1}CT energy calculated from the onset of the fluorescence is 2.58 eV. Compared with ***m*-^{t}BuTX-PTZ**, ***m*-BTX-PTZ** shows a clear redshifted fluorescence spectrum, which is attributed to the increasing electron-withdrawing ability induced by the introduction of carbonyl groups. The phosphorescence spectrum of ***m*-BTX-PTZ** in zeonex matrix is also depicted in **Figure 7**, with the onset of *ca.* 2.59 eV. It is noteworthy that the phosphorescence spectra of ***m*-BTX-PTZ** doped in zeonex and DPEPO (bis[2-(diphenylphosphino)phenyl] ether oxide) hosts show an almost identical structure (**Figure S8c**) despite the different polarities of the hosts, revealing that the triplet state of ***m*-BTX-PTZ** is an ^{3}LE state. In zeonex film, ***m*-BTX-PTZ** represents an ideal on-resonance case with a negligibly small energy gap ΔE_{ST} between ^{1}CT and ^{3}LE determined to be less than 0.01 eV, suggesting its potential as an efficient TADF emitter.

As expected, fluorescence from the ^{1}CT state of ***m*-BTX-PTZ** is visibly redshifted when dispersed in DPEPO compared to zeonex (**Figure S8c**), which results in a lower singlet state than the ^{3}LE and thus increases the ΔE_{ST}. While the fluorescence and phosphorescence spectra of both ***o*-^{t}BuTX-PTZ** and ***m*-^{t}BuTX-PTZ** show no significant differences (**Figures S8a and b**), further demonstrating their LE characters in singlet and triplet states. It is demonstrated that the presence of carbonyl groups in ***m*-BTX-PTZ** significantly increases the electron-withdrawing ability of the TX unit and thus lowers the ^{1}CT energy. On the contrary, the *tert*-butyl substituted TX acceptor in ***o*-^{t}BuTX-PTZ** and ***m*-^{t}BuTX-PTZ** is much weaker, leading to a large ΔE_{ST}. These data are also consistent with the calculations, showing that ***m*-BTX-PTZ** has an improved HOMO/LUMO separation compared with the other two compounds.

RTP Properties of ***o*-^{t}BuTX-PTZ** *and* ***m*-^{t}BuTX-PTZ**

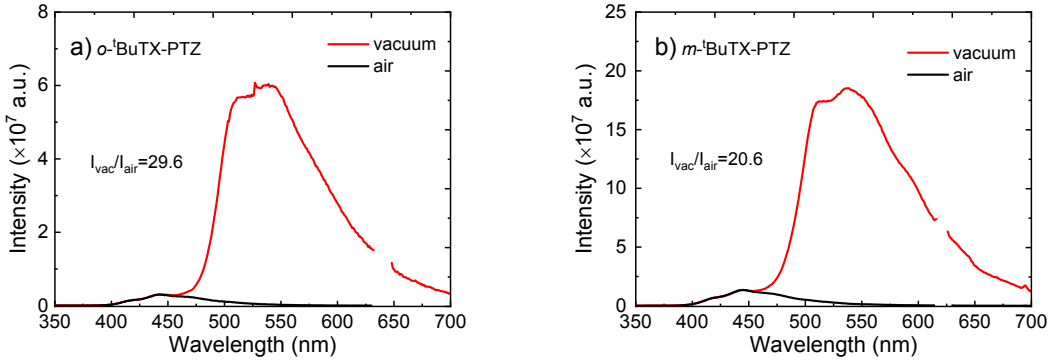

Figure 8. The steady-state emission spectra of a) ***o*-^{t}BuTX-PTZ** and b) ***m*-^{t}BuTX-PTZ** in zeonex matrix (1 wt%) in the presence (black) and absence (red) of oxygen at room temperature. The second harmonic peaks of all spectra are removed.

To better understand the influence of the substituting positions of the PTZ units on the photophysical properties, oxygen-quenching of the PL spectra of ***o*-^{t}BuTX-PTZ** and ***m*-^{t}BuTX-PTZ** in zeonex films was analyzed as shown in **Figure 8**. The emission spectra of both molecules in vacuum are dominated by phosphorescence, peaking at 540 nm. While in the presence of oxygen, the phosphorescence from the triplet state is quenched and only blue fluorescence at 450 nm is observed. The phosphorescence contributes 97% and 95% to the total emission in ***o*-^{t}BuTX-PTZ** and ***m*-^{t}BuTX-PTZ** at room temperature, respectively. This suggests that both compounds exhibit excellent RTP properties and very high triplet formation yields. Consistent with the calculations of the HOMO/LUMO distributions, the enhanced ISC in ***o*-^{t}BuTX-PTZ** results in a slightly higher triplet contribution. The photoluminescence quantum yields (PLQY) of both ***o*-^{t}BuTX-PTZ** and ***m*-^{t}BuTX-PTZ** zeonex films in aerated conditions (Φ_f = 0.008 and 0.014, respectively) are the same within experimental error. In RTP the PLQY is controlled by the competition between the radiative and non-radiative rates, both involving the triplet state and the ground-state. Both compounds show slow radiative rates for fluorescence decay (k_f~10^6 s^{-1}), which are two orders of magnitude slower than the rate of non-radiative pathways (k_{nr}^S) affecting the singlet state. Fluorescence can thus hardly compete. This explains the small fluorescence PLQY in both compounds. With the additional phosphorescence contribution in the oxygen-free condition, the PLQYs of ***o*-^{t}BuTX-PTZ** and ***m*-^{t}BuTX-PTZ** increase to 0.30 and 0.18, respectively. Strong RTP in these two molecules is associated with the large energy gap ΔE_{ST} (0.52 eV), which eliminates the possibility of the upconversion of excitons to the singlet state.

Time-resolved profiles of ***o*-^{t}BuTX-PTZ** and ***m*-^{t}BuTX-PTZ** zeonex films were collected at room temperature as depicted in **Figure S9**. Two components, prompt fluorescence (PF) and RTP, are observed in both films. ***o*-^{t}BuTX-PTZ** and ***m*-^{t}BuTX-PTZ** films show similar short-lived fluorescence (3.67 ns and 2.78 ns, respectively), which is probably due to the fast intersystem crossing (ISC) process. The prompt fluorescence of ***o*-^{t}BuTX-PTZ** and ***m*-^{t}BuTX-PTZ** zeonex films collected at an early delay time coincides with the steady-state spectra as shown in **Figures S9c** and **d**. The relatively weak phosphorescence observed at room temperature matches well with the spectra recorded at 80 K. Interestingly, when the linking position of the PTZ units is altered from *ortho*- to *meta*-positions, the phosphorescence lifetime decreases from 24.5 ms in ***o*-^{t}BuTX-PTZ** to *ca.* 7.45 ms in ***m*-^{t}BuTX-PTZ**. The short phosphorescence lifetimes in both molecules confirm the nπ* character of the excited state, which effectively facilitates the ISC between ^{1}LE and ^{3}LE. The results indicate that the triplet state of ***m*-^{t}BuTX-PTZ** is relatively more affected by non-radiative internal conversion (IC) than ***o*-^{t}BuTX-PTZ**. Both compounds show slow radiative rates for fluorescence decay (~10^6 s^{-1}), which are two orders of magnitude slower than the rate of non-radiative pathways (IC+ISC) affecting the singlet state. Fluorescence can thus hardly compete. This explains the small fluorescence PLQY in both compounds. However, the contribution of fluorescence is minimal in both compounds, therefore the triplet state should be the focus to evaluate the role of non-radiative pathways in both compounds. In solid zeonex matrix, ***o*-^{t}BuTX-PTZ** shows relative stronger PH PLQY and longer PH decay, when compared with ***m*-^{t}BuTX-PTZ**. From the PLQY of PH and the PH lifetime the product between the triplet formation yield (Φ_T) and the radiative rate of the triplet state (k_{PH}) is determined using Eq. 1. (**Table 1**). Then the non-radiative rate affecting the triplet state (k_{nr}^T) is calculated using Eq. 2 and is much faster in ***m*-^{t}BuTX-PTZ** than in ***o*-^{t}BuTX-PTZ**, which explains the weaker RTP contribution and rapid PH decay in ***m*-^{t}BuTX-PTZ**.

Table 1. Photophysical parameters of ***o*-^{t}BuTX-PTZ** and ***m*-^{t}BuTX-PTZ** in zeonex films.

	$\emptyset_F$ (%)	$\emptyset_{F+PH}$ (%)	τ_F (ns)	τ_{PH} (ms)	$k_f \times 10^6$ (s^{-1})	$k_{nr}^S \times 10^8$ (s^{-1})	$\emptyset_T k_{PH} \times 10^2$ (s^{-1})	$k_{nr}^T \times 10^2$ (s^{-1})
***o*-^{t}BuTX-PTZ**	0.8	30	3.67	24.5	2.2	2.7	0.12	0.28
***m*-^{t}BuTX-PTZ**	1.4	18	2.78	7.45	5.0	3.5	0.23	1.09

$\Phi_T k_{PH} = \frac{\Phi_{PH}}{\tau_{PH}}$ (1)

$k_{nr}^T = \tau_{PH}^{-1} - \Phi_T k_{PH}$ (2)

TADF Properties of ***m*-BTX-PTZ**

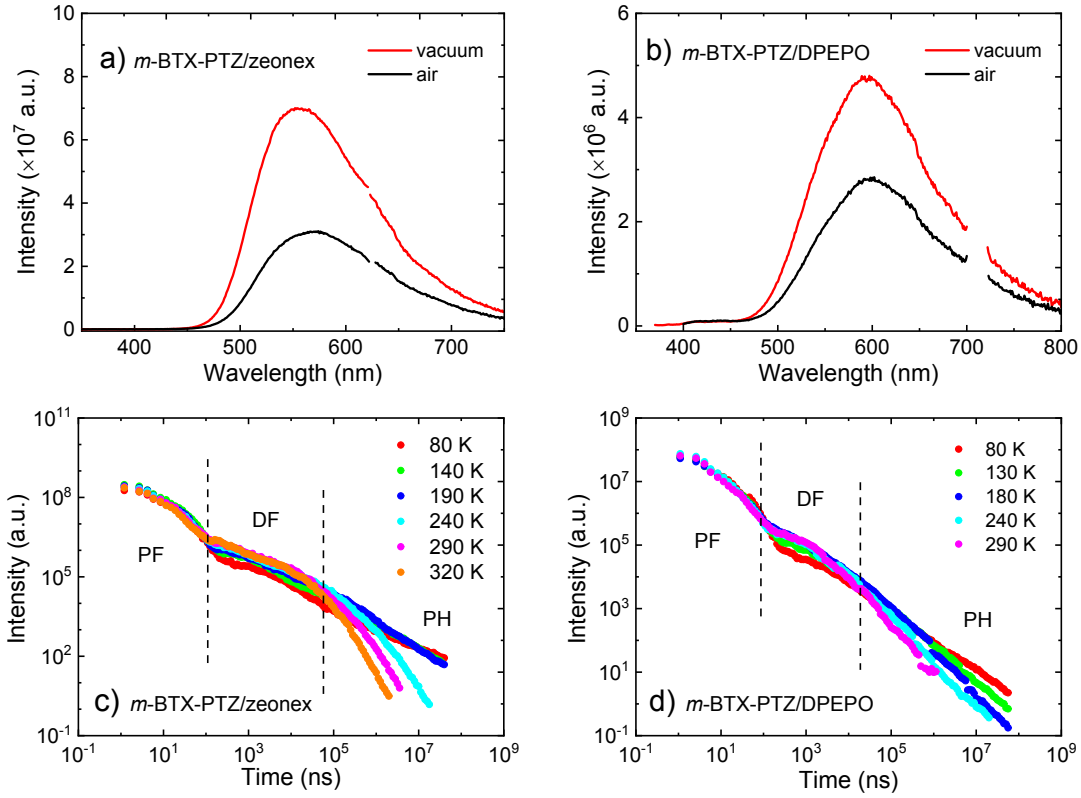

Figure 9. The steady-state emission spectra of ***m*-BTX-PTZ** in a) zeonex (1 wt%) and b) DPEPO (10%) in the presence (black) and absence (red) of oxygen at room temperature. The second harmonic peaks of all spectra are removed. Temperature dependent time-resolved decays of ***m*-BTX-PTZ** in c) zeonex and d) DPEPO.

As discussed above, the observation of RTP in ***m*-^{t}BuTX-PTZ** films is induced by the weak D/A decoupling (*i.e.* strong D/A coupling), as the acceptor strength is weaker in comparison to the strength of the donor PTZ. By introducing benzoyl groups on the TX acceptor instead of *tert*-butyl groups, the electron-withdrawing ability of ***m*-BTX-PTZ** is significantly enhanced. Owing to the small energy splitting ΔE_{ST} of 0.01 eV between ^{1}CT and ^{3}LE in ***m*-BTX-PTZ** zeonex film, excitons in the triplet state can be efficiently upconverted to the singlet state *via* RISC and TADF is observed. **Figure 9a** presents the emission spectra of ***m*-**

BTX-PTZ in zeonex matrix in the presence and absence of oxygen, showing *ca.* 54% delayed fluorescence (DF) contribution to the total emission in vacuum. The PLQY increases from 0.06 in air to 0.15 in nitrogen atmosphere. In TADF, it is mostly the competition between the RISC rate and the non-radiative rate to the ground-state that controls PLQY, as opposed to the competition between the radiative and non-radiative rates, both involving the triplet state and the ground-state, in case of RTP. Of note, similar PLQYs in the three PTZ-containing compounds indicate that the non-radiative rate between mainly the triplet and the ground-state is the main limiting factor in luminescence efficiencies. In a polar DPEPO host, the ^{1}CT state is shifted below the ^{3}LE state, which increases the ΔE_{ST} and gives rise to a smaller DF contribution compared to the zeonex films, as shown in **Figure 9b**.

To further investigate the DF mechanism of ***m*-BTX-PTZ**, temperature-dependent time-resolved measurements in zeonex and DPEPO hosts were performed. Notably, ***m*-BTX-PTZ** zeonex film exhibits clear three components (**Figure 9c**). The fast PF decay in the nanosecond range is independent of the temperature. The intensity of the DF component in the microsecond range increases with the increasing temperature as expected for a TADF mechanism. TADF is further confirmed by measurements of the emission intensity *vs* power dependence as shown in **Figure S10a**. A strictly linear proportionality of the DF intensity versus laser fluence is obtained showing that the mechanism is a monomolecular process. At even longer delay times, the decay curves show reverse temperature dependence: the emission intensity increases as the temperature decreases, which is associated with the longer-lived DF component and the increasing contribution of phosphorescence at low temperatures. Similar TADF characteristics are also observed in DPEPO host as shown in **Figures 9d** and **S10b**.

Conclusions

In this work, three new symmetrical D–A–D molecules were designed with TX as the electron acceptor unit and PTZ as electron donors, with the donor groups attached at different positions on the acceptor core – either *ortho* or *meta*. By ensuring sufficient steric hindrance, locking of the molecules in the solely equatorial conformation was realized and this strategy shows great potential in suppressing the non-radiative decay pathways.

With the *tert*-butyl substituted TX acceptor, molecules ***o*-^{t}BuTX-PTZ** and ***m*-^{t}BuTX-PTZ** show relatively large ΔE_{ST} (0.52 eV) and strong RTP is observed regardless of the donor unit PTZ substituting either on the *ortho*- or *meta*- positions. The higher degree of CT in the T_1 state of ***o*-^{t}BuTX-PTZ** leads to an enhanced π-π* character in the hybrid π-π*/n-π* orbitals. Thus, a certain amount of the CT character of the triplet state should be emphasized as an important condition for the observation of strong RTP. Unlike the reported compounds with a strong acceptor unit and well-pronounced singlet CT character, where an axial conformer was responsible for RTP and equatorial for TADF, our new RTP compounds feature a weak acceptor and CT character. Nevertheless, the weaker singlet CT state results in the formation of a singular preferable radiative pathway of the delayed emission, being the reason for the strong RTP. Furthermore, the introduction of the steric hindrance ensures necessary rigidification of the molecule in the solid state, thus facilitating strong RTP as well. The low triplet level of the PTZ unit makes the RISC rate too slow to compete with the direct deactivation of the triplet state to the ground state. Therefore, TADF is not observed even in

the equatorial conformer, which is in contrast with previously studied compounds based on dibenzothiophene-*S,S*-dioxide as the acceptor unit, and makes the distinction between axial *vs* equatorial somehow superfluous in the context of ***o*-^{t}BuTX-PTZ** and ***m*-^{t}BuTX-PTZ**. However, as for the observation of RTP it is important to suppress the non-radiative pathways that affect the triplet state other conditions become more relevant, such as i) preferably singular conformation to ensure the rigid structure; ii) rigid geometry of the T_1 state; iii) certain degree of CT in the T_1 state leading to the hybrid π-π*/n-π* orbitals.

The modification of the TX acceptor by the attachment of benzoyl substituents instead of *tert*-butyl groups strongly decouples the D and A units, leading to a very small ΔE_{ST} of < 0.01 eV between ^{1}CT and ^{3}LE states. Excitons in the triplet state can be efficiently upconverted to the singlet state *via* RISC resulting in yellow TADF. Additionally, internal *syn/anti* conformers of the PTZ unit were studied for the first time. The influence of the internal conformers of the donor on the ground and excited state properties of the target compounds has been evaluated. It has been shown that PTZ units tend to planarize in the excited state, thus making the existence of *syn/anti* conformers a solely ground state feature, which has a minor influence on the optical characteristics. This series provides new insights into how molecular functionalization and intramolecular charge transfer has profound effects on the singlet-triplet gap, ΔE_{ST}, in D–A–D molecules and the results will contribute to the future design of TADF and RTP emitters.

ASSOCIATED CONTENT

Supporting Information. The Supporting Information is available free of charge on the ACS Publications website at DOI:xxxxxxxxx

Synthesis and characterization details of the new molecules; methods and results for the photophysics and calculations (PDF). X-ray crystallographic data (CCDC 1935514-1935516); computational atomic coordinates (xyz).

AUTHOR INFORMATION

Corresponding Authors

*E-Mail: nadzeya.kukhta@durham.ac.uk

*E-Mail: m.r.bryce@durham.ac.uk

*E-Mail: f.m.b.dias@durham.ac.uk

Author Contributions

N.A.K. and R.H. contributed equally to this work. N.A.K. designed, synthesized and characterized all the compounds under the supervision of M.R.B. R.H. carried out the photophysical and electrochemical characterizations of all the compounds under the supervision of F.B.D. N.A.K. performed and analyzed all the DFT calculations. N.A.K. and R.H. lead the writing and coordination of the manuscript with additional contribution from all

the authors. A.S.B. collected X-ray diffraction data and determined crystal structures. The manuscript was read, corrected and approved by all the authors.

Notes

The authors declare no competing financial interest.

Acknowledgements

N.K. and M.R.B. thank EU Horizon 2020 Grant Agreement No. 732103 (HyperOLED) and EPSRC grant EP/L02621X/1 for funding. The Diamond Light Source (RAL) is thanked for the award of instrument time on Station I19 (MT 11145) and the instrument scientists for their kind support.

References

(1) Kuma, H.; Hosokawa, C. Blue Fluorescent OLED Materials and Their Application for High-Performance Devices. *Sci. Technol. Adv. Mater.* **2014**, *15* (3), 034201.

(2) Duan, L.; Qiao, J.; Sun, Y.; Qiu, Y. Strategies to Design Bipolar Small Molecules for OLEDs: Donor-Acceptor Structure and Non-Donor-Acceptor Structure. *Adv. Mater.* **2011**, *23* (9), 1137–1144.

(3) Bui, T.-T.; Goubard, F.; Ibrahim-Ouali, M.; Gigmes, D.; Dumur, F. Recent Advances on Organic Blue Thermally Activated Delayed Fluorescence (TADF) Emitters for Organic Light-Emitting Diodes (OLEDs). *Beilstein J. Org. Chem.* **2018**, *14*, 282–308.

(4) Reineke, S.; Lindner, F.; Schwartz, G.; Seidler, N.; Walzer, K.; Lüssem, B.; Leo, K. White Organic Light-Emitting Diodes with Fluorescent Tube Efficiency. *Nature* **2009**, *459* (7244), 234–238.

(5) Tachibana, H.; Aizawa, N.; Hidaka, Y.; Yasuda, T. Tunable Full-Color Electroluminescence from All-Organic Optical Upconversion Devices by Near-Infrared Sensing. *ACS Photonics* **2017**, *4* (2), 223–227.

(6) Wolfbeis, O. S. Sensor Paints. *Adv. Mater.* **2008**, *20* (19), 3759–3763.

(7) Pati, P. B.; Zade, S. S. Highly Emissive Triphenylamine Based Fluorophores for Detection of Picric Acid. *Tetrahedron Lett.* **2014**, *55* (38), 5290–5293.

(8) Zhang, G.; Palmer, G. M.; Dewhirst, M. W.; Fraser, C. L. A Dual-Emissive-Materials Design Concept Enables Tumour Hypoxia Imaging. *Nat. Mater.* **2009**, *8* (9), 747–751.

(9) Reineke, S.; Seidler, N.; Yost, S. R.; Prins, F.; Tisdale, W. A.; Baldo, M. A. Highly Efficient, Dual State Emission from an Organic Semiconductor. *Appl. Phys. Lett.* **2013**, *103* (9), 093302.

(10) Zhu, M.; Yang, C. Blue Fluorescent Emitters: Design Tactics and Applications in Organic Light-Emitting Diodes. *Chem. Soc. Rev.* **2013**, *42* (12), 4963.

(11) Thirion, D.; Poriel, C.; Métivier, R.; Rault-Berthelot, J.; Barrière, F.; Jeannin, O.

Violet-to-Blue Tunable Emission of Aryl-Substituted Dispirofluorene-Indenofluorene Isomers by Conformationally-Controllable Intramolecular Excimer Formation. *Chemistry* **2011**, *17* (37), 10272–10287.

(12) Monkman, A. P. Singlet Generation from Triplet Excitons in Fluorescent Organic Light-Emitting Diodes. *ISRN Mater. Sci.* **2013**, *2013*, 1–19.

(13) Earmme, T.; Jenekhe, S. A. High-Performance Multilayered Phosphorescent OLEDs by Solution-Processed Commercial Electron-Transport Materials. *J. Mater. Chem.* **2012**, *22* (11), 4660.

(14) Baldo, M. A.; O'Brien, D. F.; You, Y.; Shoustikov, A.; Sibley, S.; Thompson, M. E.; Forrest, S. R. Highly Efficient Phosphorescent Emission from Organic Electroluminescent Devices. **1998**, *395* (6698), 151–154.

(15) Chen, D.; Su, S.-J.; Cao, Y. Nitrogen Heterocycle-Containing Materials for Highly Efficient Phosphorescent OLEDs with Low Operating Voltage. *J. Mater. Chem. C* **2014**, *2* (45), 9565–9578.

(16) Jacquemin, D.; Escudero, D. The Short Device Lifetimes of Blue PhOLEDs: Insights into the Photostability of Blue Ir(Iii) Complexes. *Chem. Sci.* **2017**, *8* (11), 7844–7850.

(17) Jankus, V.; Data, P.; Graves, D.; McGuinness, C.; Santos, J.; Bryce, M. R.; Dias, F. B.; Monkman, A. P. Highly Efficient TADF OLEDs: How the Emitter-Host Interaction Controls Both the Excited State Species and Electrical Properties of the Devices to Achieve Near 100% Triplet Harvesting and High Efficiency. *Adv. Funct. Mater.* **2014**, *24* (39), 6178–6186.

(18) Nobuyasu, R. S.; Ren, Z.; Griffiths, G. C.; Batsanov, A. S.; Data, P.; Yan, S.; Monkman, A. P.; Bryce, M. R.; Dias, F. B. Rational Design of TADF Polymers Using a Donor-Acceptor Monomer with Enhanced TADF Efficiency Induced by the Energy Alignment of Charge Transfer and Local Triplet Excited States. *Adv. Opt. Mater.* **2016,** *4*, 597–607.

(19) Zhang, Q.; Li, J.; Shizu, K.; Huang, S.; Hirata, S.; Miyazaki, H.; Adachi, C. Design of Efficient Thermally Activated Delayed Fluorescence Materials for Pure Blue Organic Light Emitting Diodes. *J. Am. Chem. Soc.* **2012**, *134* (36), 14706–14709.

(20) Shizu, K.; Tanaka, H.; Uejima, M.; Sato, T.; Tanaka, K.; Kaji, H.; Adachi, C. Strategy for Designing Electron Donors for Thermally Activated Delayed Fluorescence Emitters. *J. Phys. Chem. C* **2015**, *119* (3), 1291–1297.

(21) Dias, F. B.; Santos, J.; Graves, D. R.; Data, P.; Nobuyasu, R. S.; Fox, M. A.; Batsanov, A. S.; Palmeira, T.; Berberan-Santos, M. N.; Bryce, M. R.; et al. The Role of Local Triplet Excited States and D-A Relative Orientation in Thermally Activated Delayed Fluorescence: Photophysics and Devices. *Adv. Sci.* **2016**, *3* (12), 1–10.

(22) Dias, F. B.; Penfold, T. J.; Monkman, A. P. Photophysics of Thermally Activated Delayed Fluorescence Molecules. *Methods Appl. Fluoresc.* **2017**, *5* (012001).

(23) Etherington, M. K.; Gibson, J.; Higginbotham, H. F.; Penfold, T. J.; Monkman, A. P. Revealing the Spin–vibronic Coupling Mechanism of Thermally Activated Delayed Fluorescence. *Nat. Commun.* **2016**, *7*, 13680.

(24) Gibson, J.; Monkman, A. P.; Penfold, T. J. The Importance of Vibronic Coupling for Efficient Reverse Intersystem Crossing in Thermally Activated Delayed Fluorescence

Molecules. *ChemPhysChem* **2016**, *17* (19), 2956–2961.

(25) Zhang, Q.; Li, B.; Huang, S.; Nomura, H.; Tanaka, H.; Adachi, C. Efficient Blue Organic Light-Emitting Diodes Employing Thermally Activated Delayed Fluorescence. *Nat. Photonics* **2014**, *8* (4), 326–332.

(26) Lee, I.; Lee, J. Y. Molecular Design of Deep Blue Fluorescent Emitters with 20% External Quantum Efficiency and Narrow Emission Spectrum. *Org. Electron.* **2016**, *29*, 160–164.

(27) Tanaka, H.; Shizu, K.; Miyazaki, H.; Adachi, C. Efficient Green Thermally Activated Delayed Fluorescence (TADF) from a Phenoxazine-Triphenyltriazine (PXZ-TRZ) Derivative. *Chem. Commun. (Camb).* **2012**, *48* (93), 11392–11394.

(28) Kawasumi, K.; Wu, T.; Zhu, T.; Chae, H. S.; Van Voorhis, T.; Baldo, M. A.; Swager, T. M. Thermally Activated Delayed Fluorescence Materials Based on Homoconjugation Effect of Donor-Acceptor Triptycenes. *J. Am. Chem. Soc.* **2015**, *137* (37), 11908–11911.

(29) Im, Y.; Kim, M.; Cho, Y. J.; Seo, J.-A.; Yook, K. S.; Lee, J. Y. Molecular Design Strategy of Organic Thermally Activated Delayed Fluorescence Emitters. *Chem. Mater.* **2017**, *29* (5), 1946–1963.

(30) Liu, Y.; Zhan, G.; Fang, P.; Liu, Z.; Bian, Z.; Huang, C. Manipulating Organic Triplet Harvesting in Regioisomeric Microcrystals. *J. Mater. Chem. C* **2017**, *5* (47), 12547–12552.

(31) Huang, R.; Ward, J. S.; Kukhta, N. A.; Avó, J.; Gibson, J.; Penfold, T.; Lima, J. C.; Batsanov, A. S.; Berberan-Santos, M. N.; Bryce, M. R.; et al. The Influence of Molecular Conformation on the Photophysics of Organic Room Temperature Phosphorescent Luminophores. *J. Mater. Chem. C* **2018**, *6* (34), 9238–9247.

(32) Wang, C.-R.; Gong, Y.-Y.; Yuan, W.-Z.; Zhang, Y.-M. Crystallization-Induced Phosphorescence of Pure Organic Luminogens. *Chinese Chem. Lett.* **2016**, *27* (8), 1184–1192.

(33) Forni, A.; Lucenti, E.; Botta, C.; Cariati, E. Metal Free Room Temperature Phosphorescence from Molecular Self-Interactions in the Solid State. *J. Mater. Chem. C* **2018**, *6* (17), 4603–4626.

(34) Data, P.; Takeda, Y. Recent Advancements in and the Future of Organic Emitters: TADF- and RTP-Active Multifunctional Organic Materials. *Chem. – An Asian J.* **2019**, *14* (10), 1613–1636.

(35) Ward, J. S.; Nobuyasu, R. S.; Batsanov, A. S.; Data, P.; Monkman, A. P.; Dias, F. B.; Bryce, M. R. The Interplay of Thermally Activated Delayed Fluorescence (TADF) and Room Temperature Organic Phosphorescence in Sterically-Constrained Donor–acceptor Charge-Transfer Molecules. *Chem. Commun.* **2016**, *52*, 2612–2615.

(36) Chen, C.; Huang, R.; Batsanov, A. S.; Pander, P.; Hsu, Y.-T.; Chi, Z.; Dias, F. B.; Bryce, M. R. Intramolecular Charge Transfer Controls Switching Between Room Temperature Phosphorescence and Thermally Activated Delayed Fluorescence. *Angew. Chemie* **2018**, *130* (50), 16645–16649.

(37) Tanaka, H.; Shizu, K.; Nakanotani, H.; Adachi, C. Dual Intramolecular Charge-Transfer Fluorescence Derived from a Phenothiazine-Triphenyltriazine Derivative. *J.*

Phys. Chem. C **2014**, *118* (29), 15985–15994.

(38) Huang, R.; Avó, J.; Northey, T.; Chaning-Pearce, E.; dos Santos, P. L.; Ward, J. S.; Data, P.; Etherington, M. K.; Fox, M. A.; Penfold, T. J.; et al. The Contributions of Molecular Vibrations and Higher Triplet Levels to the Intersystem Crossing Mechanism in Metal-Free Organic Emitters. *J. Mater. Chem. C* **2017**, *5* (25), 6269–6280.

(39) Wang, K.; Zheng, C.-J.; Liu, W.; Liang, K.; Shi, Y.-Z.; Tao, S.-L.; Lee, C.-S.; Ou, X.-M.; Zhang, X.-H. Avoiding Energy Loss on TADF Emitters: Controlling the Dual Conformations of D-A Structure Molecules Based on the Pseudoplanar Segments. *Adv. Mater.* **2017**, *29* (47), 1701476.

(40) Lien, Y.-J.; Lin, T.-C.; Yang, C.-C.; Chiang, Y.-C.; Chang, C.-H.; Liu, S.-H.; Chen, Y.-T.; Lee, G.-H.; Chou, P.-T.; Lu, C.-W.; et al. First N-Borylated Emitters Displaying Highly Efficient Thermally Activated Delayed Fluorescence and High-Performance OLEDs. *ACS Appl. Mater. Interfaces* **2017**, *9* (32), 27090–27101.

(41) Okazaki, M.; Takeda, Y.; Data, P.; Pander, P.; Higginbotham, H.; Monkman, A. P.; Minakata, S. Thermally Activated Delayed Fluorescent Phenothiazine-Dibenzo[a,j]Phenazine-Phenothiazine Triads Exhibiting Tricolor-Changing Mechanochromic Luminescence. *Chem. Sci.* **2017**, *8* (4), 2677–2686.

(42) Ward, J. S.; Nobuyasu, R. S.; Fox, M. A.; Batsanov, A. S.; Santos, J.; Dias, F. B.; Bryce, M. R. Bond Rotations and Heteroatom Effects in Donor-Acceptor-Donor Molecules: Implications for Thermally Activated Delayed Fluorescence and Room Temperature Phosphorescence. *J. Org. Chem.* **2018**, *83* (23), 14431-14442.

(43) Dos Santos, P. L.; Etherington, M. K.; Monkman, A. P. Chemical and Conformational Control of the Energy Gaps Involved in the Thermally Activated Delayed Fluorescence Mechanism. *J. Mater. Chem. C* **2018**, *6* (18), 4842–4853.

(44) Dos Santos, P. L.; Ward, J. S.; Bryce, M. R.; Monkman, A. P. Using Guest–Host Interactions To Optimize the Efficiency of TADF OLEDs. *J. Phys. Chem. Lett.* **2016**, *7* (17), 3341–3346.

(45) Heravi, M. M.; Kheilkordi, Z.; Zadsirjan, V.; Heydari, M.; Malmir, M. Buchwald-Hartwig Reaction: An Overview. *J. Organomet. Chem.* **2018**, *861*, 17–104.

(46) Boese, A. D.; Martin, J. M. L. Development of Density Functionals for Thermochemical Kinetics. *J. Chem. Phys.* **2004**, *121* (8), 3405–3416.

(47) Zhao, Y.; Truhlar, D. G. Density Functionals with Broad Applicability in Chemistry. *Acc. Chem. Res.* **2008**, *41* (2), 157–167.

(48) Boese, A. D.; Martin, J. M. L. Development of Novel Density Functionals for Thermochemical Kinetics. J. Chem. Phys. **2004**, *121*, 3405-3416.

(49) Kukhta, N. A.; da Silva Filho, D. A.; Volyniuk, D.; Gražulevičius, J. V.; Sini, G. Can Fluorenone-Based Compounds Emit in the Blue Region? Impact of the Conjugation Length and the Ground State Aggregation. *Chem. Mater.* **2017**, *294*, 1695-1707.

(50) Metri, N.; Sallenave, X.; Plesse, C.; Beouch, L.; Aubert, P.-H.; Goubard, F.; Chevrot, C.; Sini, G. Processable Star-Shaped Molecules with Triphenylamine Core as Hole-Transporting Materials: Experimental and Theoretical Approach. *J. Phys. Chem. C* **2012**, *116* (5), 3765–3772.

(51) Müllegger, S.; Rashidi, M.; Fattinger, M.; Koch, R. Surface-Supported Hydrocarbon π Radicals Show Kondo Behavior. *J. Phys. Chem. C* **2013**, *117* (11), 5718–5721.

(52) Chen, D. G.; Lin, T. C.; Chen, Y. A.; Chen, Y. H.; Lin, T. C.; Chen, Y. T.; Chou, P. T. Revisiting Dual Intramolecular Charge-Transfer Fluorescence of Phenothiazine-Triphenyltriazine Derivatives. *J. Phys. Chem. C* **2018**, *122* (23), 12215–12221.

(53) Sakamaki, D.; Saeki, H.; Seki, S. Synthesis and Properties of a Twin Donor Molecule Composed of Cofacially Stacked Dihydrodiazapentacenes. *Mater. Chem. Front.* **2018**, *2* (3), 530–536.

(54) Hirata, S.; Head-Gordon, M. Time-Dependent Density Functional Theory within the Tamm–Dancoff Approximation. *Chem. Phys. Lett.* **1999**, *314* (3–4), 291–299.

(55) Chantzis, A.; Laurent, A. D.; Adamo, C.; Jacquemin, D. Is the Tamm-Dancoff Approximation Reliable for the Calculation of Absorption and Fluorescence Band Shapes? *J. Chem. Theory Comput.* **2013**, *9* (10), 4517–4525.

(56) Martin, R. L. Natural Transition Orbitals. *J. Chem. Phys.* **2003**, *118* (11), 4775–4777.

(57) Zhao, W.; He, Z.; Lam, J. W. Y.; Peng, Q.; Ma, H.; Shuai, Z.; Bai, G.; Hao, J.; Tang, B. Z. Rational Molecular Design for Achieving Persistent and Efficient Pure Organic Room-Temperature Phosphorescence. *Chem* **2016**, *1* (4), 592–602.

(58) Stockmann, A.; Kurzawa, J.; Fritz, N.; Acar, N.; Schneider, S.; Daub, J.; Engl, R. ; Clark, T. Conformational Control of Photoinduced Charge Separation within Phenothiazine−Pyrene Dyads. *Phys. Chem. A* **2002**, *106* (34), 7958-7970.

(59) Xu, J.; Semin, S.; Niedzialek, D.; Kouwer, P. H. J.; Fron, E.; Coutino, E.; Savoini, M.; Li, Y.; Hofkens, J.; Uji-I, H.; et al. Self-Assembled Organic Microfibers for Nonlinear Optics. *Adv. Mater.* **2013**, *25* (14), 2084–2089.